Nuclear Physics B304 (1988) 687–711
North-Holland, Amsterdam

RADIATIVE CORRECTIONS TO BHABHA SCATTERING AT HIGH ENERGIES (I).
Virtual and soft photon corrections

M. BÖHM and A. DENNER

Physikalisches Institut, Universität Würzburg, FRG

W. HOLLIK

II. Institut für Theoretische Physik, Universität Hamburg, FRG

Received 25 August 1987
(Revised 3 February 1988)

The complete set of formulas for the differential Bhabha cross section including all the one-loop virtual corrections and soft photon bremsstrahlung emission is presented for the standard model in an on-shell renormalization scheme. The influence and structure of the corrections are discussed below, on top and around, and far above the Z^0 resonance.

1. Introduction

The high energy e^+e^- colliders LEP [1] and SLC [2] are primarily dedicated to the investigation of the electroweak interaction. In particular, from measurements in the resonance region $\sqrt{s} \approx 93$ GeV detailed information on the properties of the neutral intermediate vector boson Z^0 are expected. This provides very stringent tests of the standard model [3] of the electroweak interaction and is also a place to look for effects of possible "new physics" like extended gauge models, supersymmetry and compositeness [4]. In order to supply the precision experiments of the near future with the theoretical predictions of equivalent accuracy, radiative corrections have to be taken into account.

The process of Bhabha scattering is of prime importance at e^+e^- colliders since it serves as a reference process for luminosity measurements as well as for clean precision tests of the electroweak theory. The first calculation of the cross section for elastic e^+e^- scattering in the framework of quantum electrodynamics was performed by Bhabha [5]. Electromagnetic radiative corrections have been calculated by Readhead [6] and later also by other authors [7]. The contribution of the weak interaction to lowest order was discussed in ref. [8] for the standard model and in ref. [9] for extended gauge models with more than one Z^0 boson. One-loop

0550-3213/88/$03.50

calculations in the standard model have been done by Consoli [10] (without resonance effects) and by Consoli et al. [11] and Greco [12] (only QED corrections). Numerical results for the one-loop cross section containing real photon and all virtual corrections were given in ref. [13] and, including also hard photons, recently in ref. [14]. Numerical one-loop results without photonic corrections were also presented in ref. [15].

This is the first of two papers in which the standard model one-loop corrections to $e^+e^- \to e^+e^-$ are described in detail with respect to their application in realistic experiments. In the present paper we have collected the formulae for the purely weak corrections and the virtual and real electromagnetic corrections in the soft photon limit, including the resonance effect in the initial-state radiation. The calculation was performed in the on-shell renormalization scheme described in ref. [16]. The hard photon part will be treated in the subsequent publication [17], where the analytic results of this paper provide the (inclusive) two-particle cross section of a complete Monte Carlo program.

We discuss the importance of the weak and soft QED part in this paper at energies well below M_Z, around the Z^0 and far above the resonance up to 1 TeV. The analytic formulae given here allow also an easy approximate calculation of the one-loop Bhabha cross section if the cuts to the emitted photon energy are not too high (typically $\Delta E_\gamma / E_{\text{beam}} \lesssim 0.1$ or acollinearity cuts with $\delta_{\text{acoll}} \lesssim 7^0$). A rigorous discussion, however, is possible only after a combination of the two parts in one program.

In sect. 2 we set up our notation and put together the lowest order cross section including longitudinal polarization of the electrons and positrons. The electromagnetic corrections are given in sect. 3, the weak corrections in sect. 4. Numerical results for the differential cross section are presented and discussed in sect. 5.

2. Notation, lowest order cross section

We discuss in the framework of the standard model [3] Bhabha scattering at high energies ($s \gg m_e^2$). We use, for the incoming and outgoing electrons and positrons, helicity states [18] with polarizations $\lambda_{\mp}$, $\Lambda_{\mp}$, the scattering angle is denoted by θ. In this context it is convenient to work with left- and right-handed couplings g_λ of the vector bosons ($\gamma, Z, W^{\pm}$) to the electron:

$$
\begin{aligned}
g_-^\gamma &= 1, & g_+^\gamma &= 1, \\
g_-^Z &= \frac{2s_w^2 - 1}{2s_w c_w}, & g_+^Z &= \frac{s_w}{c_w}, \\
g_-^W &= \frac{1}{\sqrt{2}\, s_w}, & g_+^W &= 0.
\end{aligned}
\tag{2.1}
$$

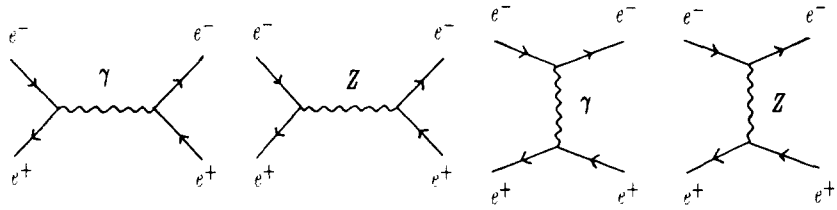

Fig. 1. Born matrix elements.

The weak mixing angle θ_w is a shorthand in the on-shell scheme

$$\cos\theta_w = c_w = \frac{M_W}{M_Z}, \qquad s_w = \sqrt{1 - c_w^2}\,. \tag{2.2}$$

The lowest order helicity amplitudes $\mathcal{M}_0(\lambda_-, \lambda_+, \Lambda_-, \Lambda_+)$ get contributions from s- and t-channel exchange of the photon and the Z^0-boson (fig. 1) denoted by $\mathcal{M}_0^{ri}(\lambda_-, \lambda_+, \Lambda_-, \Lambda_+)$ $(r = s, t;\ i = \gamma, Z)$

$$\mathcal{M}_0(\lambda_-, \lambda_+, \Lambda_-, \Lambda_+) = \sum_{i,r} \mathcal{M}_0^{ri}(\lambda_-, \lambda_+, \Lambda_-, \Lambda_+)\,. \tag{2.3}$$

Since the Higgs–electron coupling is proportional to the electron mass m_e we can neglect the Higgs exchange diagrams. For high energies $s \gg m_e^2$, due to helicity selection rules the only non-vanishing contributions are

$$\begin{aligned}
\mathcal{M}_0^{si}(\lambda, -\lambda, \lambda, -\lambda) &= \mathcal{M}_1^{si}(\lambda) = 2\frac{u}{s} g_\lambda^i \chi^i(s) g_\lambda^i\,,\\
\mathcal{M}_0^{si}(\lambda, -\lambda, -\lambda, \lambda) &= \mathcal{M}_2^{si}(\lambda) = 2\frac{t}{s} g_\lambda^i \chi^i(s) g_{-\lambda}^i\,,\\
\mathcal{M}_0^{ti}(\lambda, -\lambda, \lambda, -\lambda) &= \mathcal{M}_1^{ti}(\lambda) = 2\frac{u}{t} g_\lambda^i \chi^i(t) g_\lambda^i\,,\\
\mathcal{M}_0^{ti}(\lambda, \lambda, \lambda, \lambda) &= \mathcal{M}_3^{ti}(\lambda) = 2\frac{s}{t} g_\lambda^i \chi^i(t) g_{-\lambda}^i\,,
\end{aligned} \tag{2.4}$$

where the reduced propagators $\chi^i(s)$ are given by

$$\begin{aligned}
\chi^\gamma(s) &= \chi^\gamma(t) = 1\,,\\
\chi^Z(s) &= \frac{s}{s - M^2} = \frac{s}{s - M_Z^2 + iM_Z\Gamma_Z}\,,\\
\chi^Z(t) &= \frac{t}{t - M_Z^2}\,.
\end{aligned} \tag{2.5}$$

Squaring of the matrix elements yields the Born cross section

$$\frac{4s}{\alpha^2}\left(\frac{d\sigma}{d\Omega}\right)_{a,\mathrm{Born}}(\lambda)=\left|\sum_{i,r}\mathscr{M}_a^{ri}(\lambda)\right|^2. \tag{2.6}$$

The cross section with arbitrary degree $P^{\pm}$ of longitudinal polarization of the incoming electrons and positrons and summed over the final helicities has the general form:

$$\left(\frac{d\sigma}{d\Omega}\right)(P^+,P^-)=\left(\frac{d\sigma}{d\Omega}\right)_{\mathrm{U}}(1-P^+P^-)+(P^+-P^-)\left(\frac{d\sigma}{d\Omega}\right)_{\mathrm{L}}+P^+P^-\left(\frac{d\sigma}{d\Omega}\right)_{\mathrm{LL}}, \tag{2.7}$$

with

$$\left(\frac{d\sigma}{d\Omega}\right)_{\mathrm{U}}=\tfrac{1}{4}\sum_{\lambda,a}\left(\frac{d\sigma}{d\Omega}\right)_a(\lambda),$$

$$\left(\frac{d\sigma}{d\Omega}\right)_{\mathrm{L}}=-\tfrac{1}{4}\sum_{\lambda}\lambda\left(\frac{d\sigma}{d\Omega}\right)_1(\lambda),$$

$$\left(\frac{d\sigma}{d\Omega}\right)_{\mathrm{LL}}=\tfrac{1}{2}\sum_{\lambda}\left(\frac{d\sigma}{d\Omega}\right)_3(\lambda). \tag{2.8}$$

In the Born approximation these read

$$\frac{s}{\alpha^2}\left(\frac{d\sigma}{d\Omega}\right)_{\mathrm{U}}=\frac{1}{2}\left[\frac{u^2}{s^2}A_{\mathrm{U}}(s,s)+\frac{u^2}{t^2}A_{\mathrm{U}}(t,t)+\frac{2u^2}{ts}A_{\mathrm{U}}(t,s)\right.$$
$$\left.+\frac{t^2}{s^2}B_{\mathrm{U}}(s,s)+\frac{s^2}{t^2}B_{\mathrm{U}}(t,t)\right],$$

$$\frac{s}{\alpha^2}\left(\frac{d\sigma}{d\Omega}\right)_{\mathrm{L}}=\frac{1}{2}\left[\frac{u^2}{s^2}A_{\mathrm{L}}(s,s)+\frac{u^2}{t^2}A_{\mathrm{L}}(t,t)+\frac{2u^2}{st}A_{\mathrm{L}}(t,s)\right],$$

$$\frac{s}{\alpha^2}\left(\frac{d\sigma}{d\Omega}\right)_{\mathrm{LL}}=\frac{s^2}{t^2}B_{\mathrm{U}}(t,t), \tag{2.9}$$

with

$$A_U(t,s) = 1 + \frac{g_-^2 + g_+^2}{2}\mathrm{Re}\{\chi^*(t) + \chi(s)\} + \frac{g_-^4 + g_+^4}{2}\mathrm{Re}\{\chi^*(t)\chi(s)\},$$

$$A_L(t,s) = \frac{g_-^2 - g_+^2}{2}\mathrm{Re}\{\chi^*(t) + \chi(s)\} + \frac{g_-^4 - g_+^4}{2}\mathrm{Re}\{\chi^*(t)\chi(s)\},$$

$$B_U(t,s) = 1 + g_+ g_- \mathrm{Re}\{\chi^*(t) + \chi(s)\} + g_+^2 g_-^2 \mathrm{Re}\{\chi^*(t)\chi(s)\}, \qquad (2.10)$$

where the contributions from the photon exchange, the photon–Z-boson interference and the Z-boson exchange are separated. In pure QED A_U and B_U equal 1, whereas A_L vanishes.

3. Electromagnetic corrections (excluding hard bremsstrahlung)

For the calculation of radiative corrections a specification of the renormalization scheme is needed. We use the on-shell renormalization scheme [16] with the fine-structure constant α and masses M_W, M_Z, M_H and m_f as physical parameters. It is constructed in such a way that on-shell photons ($k^2 = 0$) are decoupled from the Z, which means that QED is realized as substructure in the usual way. Consequently, we split up the one-loop radiative corrections into electromagnetic and weak ones. The virtual corrections i.e. self-energy, vertex and box-diagram corrections of the standard model factorize for high energies ($s, |t|, |u| \gg m_e^2$) into the lowest order matrix elements and correction terms

$$\mathcal{M}^{ri}_{a,\mathrm{virt}}(\lambda) = \mathcal{M}^{ri}_a(\lambda)\,\delta^{ri}_a(\lambda) = \mathcal{M}^{ri}_a(\lambda)\left[\delta^{ri}_{a,\mathrm{em}}(\lambda) + \delta^{ri}_{a,\mathrm{weak}}(\lambda)\right]. \qquad (3.1)$$

In this section we summarize the electromagnetic corrections to the Bhabha cross section to order α^3. Among these there are one-loop diagrams which possess after UV-renormalization still infrared-divergent parts. These are regularized by a small photon mass μ and are compensated by real photon emission which, in this section, will be treated in the soft photon approximation taking into account photons up to an energy $\Delta E \ll \sqrt{s}$. The additional contributions of hard photons will be treated in the subsequent publication [17].

3.1. VIRTUAL ELECTROMAGNETIC CORRECTIONS

The virtual electromagnetic corrections consist of the corrections due to virtual photons and of fermion loop corrections to the photon self-energy.

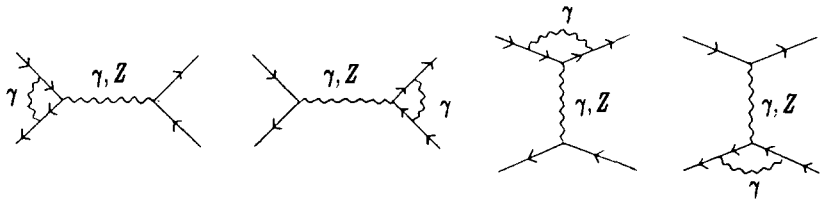

Fig. 2. Electromagnetic vertex corrections.

(a) The photonic *vertex corrections* [19] of fig. 2 yield (μ is the photon mass)

$$\delta^{ri}_{a,\mathrm{em,V}}(\lambda) = 2F_{\mathrm{em}}(r) = \frac{\alpha}{2\pi}\left\{-2\ln\frac{-r}{\mu^2-i\varepsilon}\left(\ln\frac{-r}{m_e^2-i\varepsilon}-1\right)+\ln\frac{-r}{m_e^2-i\varepsilon}\right.$$

$$\left.+\left(\ln\frac{-r}{m_e^2-i\varepsilon}\right)^2+\frac{\pi^2}{3}-4\right\}. \quad (3.2)$$

(b) The result for the $\gamma\gamma$-*box diagrams* [20] (fig. 3) is*

$$\delta^{s\gamma}_{\substack{1\\2},\mathrm{em,B}}(\lambda) = C^{\gamma\gamma}_{\pm}(s,t),$$

$$\delta^{t\gamma}_{\substack{1\\3},\mathrm{em,B}}(\lambda) = C^{\gamma\gamma}_{\pm}(t,s), \quad (3.3)$$

with

$$C^{\gamma\gamma}_{\pm}(s,t) = \frac{\alpha}{2\pi}\left\{-2\ln\left(\frac{t}{u}-i\varepsilon\right)\ln\left(\frac{-s}{\mu^2}-i\varepsilon\right)\right\} \pm 2I_5^{\gamma\gamma}\left(s,{}^{t}_{u}\right) \quad (3.4)$$

and for the γZ-box diagrams [21] (fig. 4)

$$\delta^{sZ}_{\substack{1\\2},\mathrm{em,B}}(\lambda) = C^{\gamma Z}_{\pm}(s,t),$$

$$\delta^{tZ}_{\substack{1\\3},\mathrm{em,B}}(\lambda) = C^{\gamma Z}_{\pm}(t,s), \quad (3.5)$$

* Here and in the following we combine two formulae into one. The upper and the lower of the indices $\frac{1}{2}$ or of the arguments ${}^{t}_{u}$ belong to the upper and lower sign $\pm$, respectively.

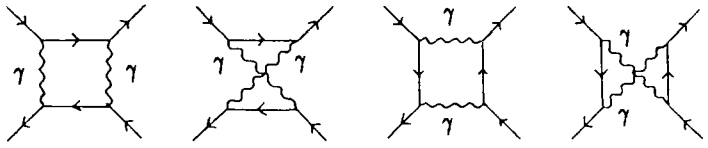

Fig. 3. γγ-box diagrams.

with

$$C_{\pm}^{\gamma Z}(s,t)=\frac{\alpha}{2\pi}\left\{-2\ln\left(\frac{t}{u}-i\varepsilon\right)\left[\ln\left(\frac{M^2-s}{\mu^2}\right)+\ln\left(\frac{M^2-s}{M^2}\right)\right]\right.$$
$$\left.+2\,\mathrm{Sp}\left(\frac{M^2+t}{t}\right)-2\,\mathrm{Sp}\left(\frac{M^2+u}{u}\right)\right\}\pm 4I_5^{\gamma Z}\left(s,{}^{t}_{u}\right),$$

$$C_{\pm}^{\gamma Z}(t,s)=\frac{\alpha}{2\pi}\left\{-2\ln\left(\frac{s}{u}-i\varepsilon\right)\left[\ln\left(\frac{M_Z^2-t}{\mu^2}\right)+\ln\left(\frac{M_Z^2-t}{M_Z^2}\right)\right]\right.$$
$$\left.+2\,\mathrm{Sp}\left(\frac{M_Z^2+s}{s}\right)-2\,\mathrm{Sp}\left(\frac{M_Z^2+u-i\varepsilon}{u}\right)\right\}\pm 4I_5^{\gamma Z}\left(t,{}^{s}_{u}\right). \qquad (3.6)$$

The Spence function [22] is defined by $\mathrm{Sp}(x)=-\int_0^1(\mathrm{d}t/t)\ln(1-xt)$. $I_5^{\gamma\gamma}$ and $I_5^{\gamma Z}$ are given in the appendix of ref. [16].

(c) In our renormalization scheme we do not need wave-function renormalization for electrons and positrons, therefore the only electromagnetic *self-energy corrections* are the fermionic contributions to the photon self-energy [19] (fig. 5). The corresponding correction factors $\delta_{a,\mathrm{em},\Sigma}^{ri}(\lambda)$ read

$$\delta_{a,\mathrm{em},\Sigma}^{r\gamma}(\lambda)=\Pi_{\mathrm{em,lept}}^{\gamma}(r)+\Pi_{\mathrm{em,had}}^{\gamma}(r),$$
$$\delta_{a,\mathrm{em},\Sigma}^{rZ}(\lambda)=0. \qquad (3.7)$$

The leptonic part is given by

$$\Pi_{\mathrm{em,lept}}^{\gamma}(r)=-\hat{\Sigma}_{\mathrm{em,lept}}^{\gamma}(r)/r=\frac{\alpha}{2\pi}\sum_{\ell}Q_{\ell}^2\left[\frac{2}{9}-\frac{2}{3}\left(1+\frac{2m_{\ell}^2}{r}\right)F(r,m_{\ell},m_{\ell})\right], \qquad (3.8)$$

where the sum extends over all charged leptons with charges Q_{ℓ} and masses m_{ℓ}. The scalar function F is defined in ref. [16].

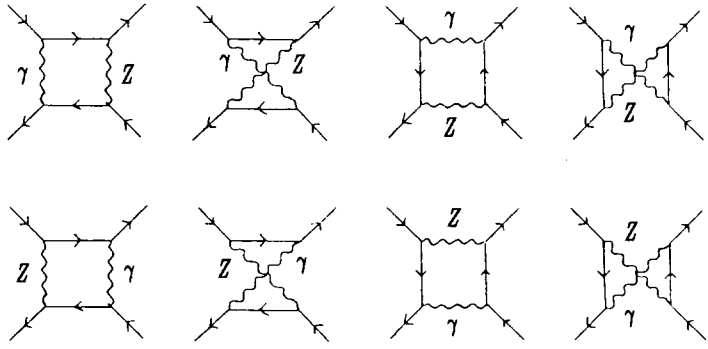

Fig. 4. γZ-box diagrams.

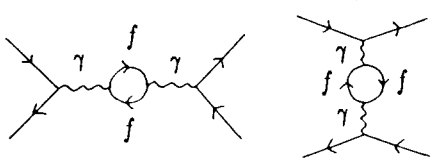

Fig. 5. Electromagnetic self-energy corrections.

The hadronic part $\Pi^{\gamma}_{\mathrm{em,had}}$ includes the light quark contributions where nonperturbative strong-interaction effects cannot be ignored. Since reliable theoretical predictions are not available for these contributions, one has to use experimental data for their evaluation. The real part satisfies the dispersion relation

$$\mathrm{Re}\,\Pi^{\gamma}_{\mathrm{em,had}}(r) = \frac{\alpha}{3\pi} r \int_{4m_\pi^2}^{\infty} \mathrm{d}s \, \frac{R^{\gamma\gamma}(s)}{s(s - r - i\varepsilon)}, \tag{3.9}$$

with

$$R^{\gamma\gamma}(s) = \frac{\sigma(\mathrm{e}^+\mathrm{e}^- \to \gamma^* \to \mathrm{hadrons})}{\sigma(\mathrm{e}^+\mathrm{e}^- \to \gamma^* \to \mu^+\mu^-)}, \tag{3.10}$$

as a fairly well-known experimental quantity as input. The evaluation of this integral for 5 flavours using $\mathrm{e}^+\mathrm{e}^-$ data up to an energy E_1 and perturbative field theory for the tail $E > E_1$ was recently updated by Jegerlehner [23] (for earlier work see ref. [24]). Around the weak boson mass scale the result for $\Pi^{\gamma}_{\mathrm{em,had}}$ can be described sufficiently well in analytical form by an expression which is equivalent to the result of a perturbative calculation with quark loop diagrams [23,25] yielding a result similar to our (3.8). The quark mass parameters are effective quark masses adjusted to fit the numerical value for the dispersion integral. The values which

reproduce the result of [23] are

$$m_u = m_d = 32\ \text{MeV}, \qquad m_s = 150\ \text{MeV},$$
$$m_c = 1.5\ \text{GeV}, \qquad m_b = 4.5\ \text{GeV}. \tag{3.11}$$

The same vacuum polarization term $\Pi^{\gamma}_{\text{em,had}}$ appears in the fermionic contribution to the real part of the renormalized Z-boson self-energy Σ_Z (sect. 4), which together with the lepton contribution is the dominant part of Σ_Z. Replacing the terms with large logarithms $\sim \Sigma_{q \neq t} Q_q^2 \log(s/m_q^2)$ in the perturbatively obtained expression for Σ_Z from [16] by the dispersion integral leaves only terms of $O(m_q^2/M_W^2)$ which would vanish in the limit $m_q \to 0$. Therefore, for the case of light fermions only, the fermionic contribution to the weak boson self-energy reduces to that of the QED correction of the photon propagator.

For the values of the light quark masses specified above, the finite-mass terms are completely unimportant; thus our lack of understanding of those masses is no obstacle for practical applications. The uncertainty connected with the light hadron contributions is the uncertainty in the e^+e^- data, estimated to be ± 0.0007 [23] and ± 0.0013 [24], respectively.

The b, t quark contribution has been calculated perturbatively with free quark masses. For large m_t the quadratic terms $\sim m_t^2/M_W^2$ give rise to big effects in the weak vector boson 2-point functions which are different from the QED corrections in the photon propagator. For example, for the parameters specified in sect. 5, the corrections in the real part of the Z propagator are reduced by 4% if m_t is shifted from 40 to 200 GeV.

The contribution to the cross section from these virtual corrections is given by

$$\delta\left(\frac{d\sigma}{d\Omega}\right)_{a,\text{em,virt}}(\lambda)$$
$$= \frac{\alpha^2}{4s} \sum_{r,i,r',i'} \text{Re}\left\{ \mathcal{M}_a^{ri}(\lambda) \mathcal{M}_a^{r'i'*}(\lambda) \left[\delta^{ri}_{a,\text{em,virt}}(\lambda) + \delta^{r'i'*}_{a,\text{em,virt}}(\lambda) \right] \right\}, \tag{3.12}$$

where

$$\delta^{ri}_{a,\text{em,virt}}(\lambda) = \delta^{ri}_{a,\text{em},\Sigma}(\lambda) + \delta^{ri}_{a,\text{em,V}}(\lambda) + \delta^{ri}_{a,\text{em,B}}(\lambda). \tag{3.13}$$

3.2. SOFT PHOTON BREMSSTRAHLUNG

The Feynman diagrams (fig. 6) for the nonresonant emission of a photon with momentum k and polarization vector $\varepsilon^{\mu}(k,\sigma)$ give, in the limit of small photon energy k_0 [19],

$$\mathcal{M}^{\text{NR}}_{a,\text{Brems}}(\lambda) = \left[\mathcal{M}^{s\gamma}_a(\lambda) + \mathcal{M}^{t\gamma}_a(\lambda) + \mathcal{M}^{tZ}_a(\lambda) \right] \mathcal{J}^{\text{NR}}_{\mu}(k) \varepsilon^{\mu}(k,\sigma) (2\pi)^{-3/2}, \tag{3.14}$$

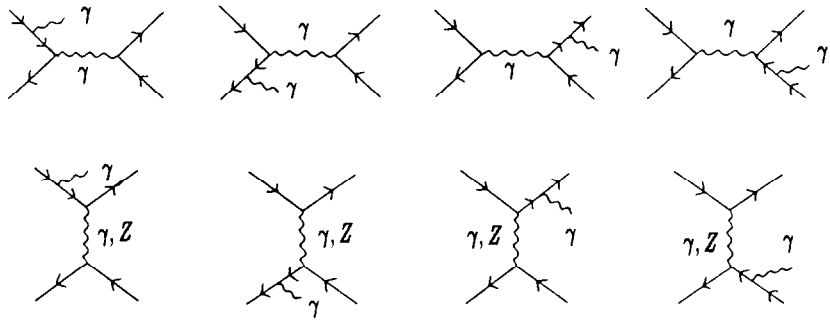

Fig. 6. Nonresonant bremsstrahlung diagrams.

with the electromagnetic current

$$\mathscr{J}_\mu^{\mathrm{NR}}(k) = -e\left[\frac{p_{-\mu}}{p_-k} - \frac{p_{+\mu}}{p_+k} - \frac{q_{-\mu}}{q_-k} + \frac{q_{+\mu}}{q_+k}\right]. \tag{3.15}$$

The emission of a bremsstrahlung quantum from the resonant scattering (fig. 7) leads to the expression [26]

$$\mathscr{M}_{a,\mathrm{Brems}}^{\mathrm{Res}}(\lambda) = \mathscr{M}_a^{sZ}(\lambda)\mathscr{J}_\mu^{\mathrm{Res}}(k)\varepsilon^\mu(k,\sigma)(2\pi)^{-3/2}, \tag{3.16}$$

with

$$\mathscr{J}_\mu^{\mathrm{Res}}(k) = -e\left[\left(\frac{p_{-\mu}}{p_-k} - \frac{p_{+\mu}}{p_+k}\right)\frac{s-M^2}{s-M^2-2k_0\sqrt{s}} - \frac{q_{-\mu}}{q_-k} + \frac{q_{+\mu}}{q_+k}\right]. \tag{3.17}$$

The factor multiplying emission from the initial state takes account of the energy shift due to photon emission in the resonant matrix element.

The soft photon cross section is obtained by squaring $\mathscr{M}_{\mathrm{Brems}}$ and integrating over the photon phase space with $|\boldsymbol{k}| < \Delta E$

$$\left(\frac{\mathrm{d}\sigma}{\mathrm{d}\Omega}\right)_{a,\mathrm{Brems}}^{\mathrm{NR}}(\lambda) = \frac{\alpha^2}{4s}\int_{|\boldsymbol{k}|<\Delta E}\frac{\mathrm{d}^3k}{2k_0}\left|\mathscr{M}_{a,\mathrm{Brems}}^{\mathrm{NR}}(\lambda)\right|^2 = \left(\frac{\mathrm{d}\sigma}{\mathrm{d}\Omega}\right)_a^{\mathrm{NR}}(\lambda)\,\delta^{\mathrm{NR}},$$

$$\left(\frac{\mathrm{d}\sigma}{\mathrm{d}\Omega}\right)_{a,\mathrm{Brems}}^{\mathrm{Int}}(\lambda) = \frac{\alpha^2}{4s}\int_{|\boldsymbol{k}|<\Delta E}\frac{\mathrm{d}^3k}{2k_0}2\,\mathrm{Re}\left\{\mathscr{M}_{a,\mathrm{Brems}}^{\mathrm{NR}*}(\lambda)\mathscr{M}_{a,\mathrm{Brems}}^{\mathrm{Res}}(\lambda)\right\}$$

$$= 2\,\mathrm{Re}\left\{\left[\mathscr{M}_a^{s\gamma}(\lambda) + \mathscr{M}_a^{t\gamma}(\lambda) + \mathscr{M}_a^{tZ}(\lambda)\right]^*\mathscr{M}_a^{sZ}(\lambda)\,\delta^{\mathrm{int}}\right\},$$

$$\left(\frac{\mathrm{d}\sigma}{\mathrm{d}\Omega}\right)_{a,\mathrm{Brems}}^{\mathrm{Res}}(\lambda) = \frac{\alpha^2}{4s}\int_{|\boldsymbol{k}|<\Delta E}\frac{\mathrm{d}^3k}{2k_0}\left|\mathscr{M}_{a,\mathrm{Brems}}^{\mathrm{Res}}(\lambda)\right|^2 = \left(\frac{\mathrm{d}\sigma}{\mathrm{d}\Omega}\right)_a^{\mathrm{Res}}(\lambda)\,\delta^{\mathrm{Res}}, \tag{3.18}$$

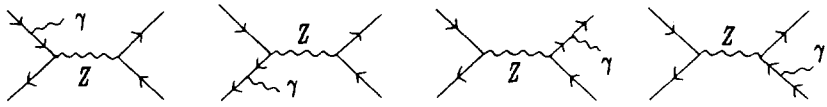

Fig. 7. Resonant bremsstrahlung diagrams.

with

$$\delta^{\mathrm{NR}} = \frac{\alpha}{\pi}\left\{4\beta_{\mathrm{e}}\ln\frac{2\Delta E}{\mu} + 4\beta_{\mathrm{int}}\ln\frac{2\Delta E}{\mu} - \beta_{\mathrm{e}}^2 + 1 - \tfrac{2}{3}\pi^2 + X\right\},$$

$$\delta^{\mathrm{Int}} = \delta^{\mathrm{NR}} + \frac{\alpha}{\pi}\left\{2\beta_{\mathrm{e}}\ln\frac{M^2 - s}{M^2 - s + 2\sqrt{s}\,\Delta E} + 2\beta_{\mathrm{int}}\ln\frac{M^2 - s}{M^2 - s + 2\sqrt{s}\,\Delta E}\right\},$$

$$\delta^{\mathrm{Res}} = \delta^{\mathrm{NR}} + \frac{\alpha}{\pi}\left\{2\beta_{\mathrm{e}}\ln\left|\frac{M^2 - s}{M^2 - s + 2\sqrt{s}\,\Delta E}\right| + 4\beta_{\mathrm{int}}\ln\left|\frac{M^2 - s}{M^2 - s + 2\sqrt{s}\,\Delta E}\right| + 2\beta_{\mathrm{e}}\frac{s - M_{\mathrm{Z}}^2}{M_{\mathrm{Z}}\Gamma_{\mathrm{Z}}}(\Phi - \Phi_0)\right\}, \quad (3.19)$$

$$\beta_{\mathrm{e}} = \ln\frac{s}{m_{\mathrm{e}}^2} - 1, \qquad \beta_{\mathrm{int}} = \ln\frac{t}{u}, \quad (3.20)$$

$$X = 2\,\mathrm{Sp}\left(-\frac{u}{s}\right) - \left(\ln\frac{-u}{s}\right)^2 - 2\,\mathrm{Sp}\left(-\frac{t}{s}\right) + \left(\ln\frac{-t}{s}\right)^2, \quad (3.21)$$

$$\Phi = \arctan\frac{M_{\mathrm{Z}}^2 - s + 2\sqrt{s}\,\Delta E}{M_{\mathrm{Z}}\Gamma_{\mathrm{Z}}}, \qquad \Phi_0 = \arctan\frac{M_{\mathrm{Z}}^2 - s}{M_{\mathrm{Z}}\Gamma_{\mathrm{Z}}}. \quad (3.22)$$

3.3. CROSS SECTION INCLUDING ELECTROMAGNETIC CORRECTIONS TO ORDER α^3

Summing the virtual (3.12) and bremsstrahlung contribution (3.18) gives the electromagnetic radiative corrections to the Bhabha cross section

$$\begin{aligned}\delta\left(\frac{\mathrm{d}\sigma}{\mathrm{d}\Omega}\right)_{a,\mathrm{em}}(\lambda) &= \delta\left(\frac{\mathrm{d}\sigma}{\mathrm{d}\Omega}\right)_{a,\mathrm{em,virt}}(\lambda) + \left(\frac{\mathrm{d}\sigma}{\mathrm{d}\Omega}\right)_{a,\mathrm{Brems}}(\lambda)\\ &= \sum_{r,i;\,r',i' \neq \mathrm{s,Z}} \mathrm{Re}\left\{\mathscr{M}_a^{ri}(\lambda)^*\mathscr{M}_a^{r'i'}(\lambda)\left[\delta_{a,\mathrm{em}}^{ri}(\lambda)^* + \delta_{a,\mathrm{em}}^{r'i'}(\lambda) + \gamma^{\mathrm{NR}}\right]\right\}\\ &\quad + 2\sum_{r,i \neq \mathrm{s,Z}} \mathrm{Re}\left\{\mathscr{M}_a^{ri}(\lambda)^*\mathscr{M}_a^{\mathrm{sZ}}(\lambda)\left[\delta_{a,\mathrm{em}}^{ri}(\lambda)^* + \delta_{a,\mathrm{em}}^{\mathrm{sZ}}(\lambda) + \gamma^{\mathrm{Int}}\right]\right\}\\ &\quad + \mathrm{Re}\left\{\mathscr{M}_a^{\mathrm{sZ}}(\lambda)^*\mathscr{M}_a^{\mathrm{sZ}}(\lambda)\left[\delta_{a,\mathrm{em}}^{\mathrm{sZ}}(\lambda)^* + \delta_{a,\mathrm{em}}^{\mathrm{sZ}}(\lambda) + \gamma^{\mathrm{Res}}\right]\right\}.\end{aligned} \quad (3.23)$$

It is infrared finite but depends on the allowed photon energy ΔE. The explicit expressions for the terms occurring in (3.23) read

$$\delta_{1,\mathrm{em}}^{s\gamma}(\lambda) = \Pi_{\mathrm{em}}^{\gamma}(s) + \frac{\alpha}{2\pi}\left[Z + X \pm 2I_5^{\gamma\gamma}\left(s, {}^{t}_{u}\right)\right],$$

$$\delta_{1,\mathrm{em}}^{t\gamma}(\lambda) = \Pi_{\mathrm{em}}^{\gamma}(t) + \frac{\alpha}{2\pi}\left[Z + Y + X \pm 2I_5^{\gamma\gamma}\left(t, {}^{s}_{u}\right)\right],$$

$$\delta_{1,\mathrm{em}}^{sZ}(\lambda) = \frac{\alpha}{2\pi}\left[Z + X \pm 4I_5^{\gamma Z}\left(s, {}^{t}_{u}\right) + 2D(s,t)\right],$$

$$\delta_{1,\mathrm{em}}^{tZ}(\lambda) = \frac{\alpha}{2\pi}\left[Z + Y + X \pm 4I_5^{\gamma Z}\left(t, {}^{s}_{u}\right) + 2D(t,s)\right], \tag{3.24}$$

where

$$Z = 3\ln\left(\frac{s}{m_e^2}\right) + \frac{2\pi^2}{3} - 4,$$

$$Y = 3\ln\frac{-t}{s} - \left(\ln\frac{-t}{s}\right)^2 - \pi^2 + 2\ln\frac{-u}{s}\ln\frac{-t}{s} + 2\pi i\left(\ln\frac{-u}{s} + \tfrac{3}{2}\right),$$

$$D(s,t) = -\ln\left(\frac{t}{u} - i\varepsilon\right)\left[\ln\left(\frac{M^2 - s}{-s}\right) + \ln\left(\frac{M^2 - s}{M^2}\right)\right] + 2\,\mathrm{Sp}\left(\frac{M^2 + t}{t}\right) - 2\,\mathrm{Sp}\left(\frac{M^2 + u}{u}\right), \tag{3.25}$$

and

$$\gamma^{\mathrm{NR}} = 4\frac{\alpha}{\pi}\ln\frac{2\Delta E}{\sqrt{s}}(\beta_e + \beta_{\mathrm{int}}),$$

$$\gamma^{\mathrm{Int}} = \gamma^{\mathrm{NR}} + 2\frac{\alpha}{\pi}\left\{\beta_e \ln\frac{M^2 - s}{M^2 - s + 2\sqrt{s}\,\Delta E} + \beta_{\mathrm{int}}\ln\frac{M^2 - s}{M^2 - s + 2\sqrt{s}\,\Delta E}\right\},$$

$$\gamma^{\mathrm{Res}} = \gamma^{\mathrm{NR}} + 2\frac{\alpha}{\pi}\left\{\beta_e \ln\left|\frac{M^2 - s}{M^2 - s + 2\sqrt{s}\,\Delta E}\right| + 2\beta_{\mathrm{int}}\ln\left|\frac{M^2 - s}{M^2 - s + 2\sqrt{s}\,\Delta E}\right| + \beta_e\frac{s - M_Z^2}{M_Z\Gamma_Z}(\Phi - \Phi_0)\right\}. \tag{3.26}$$

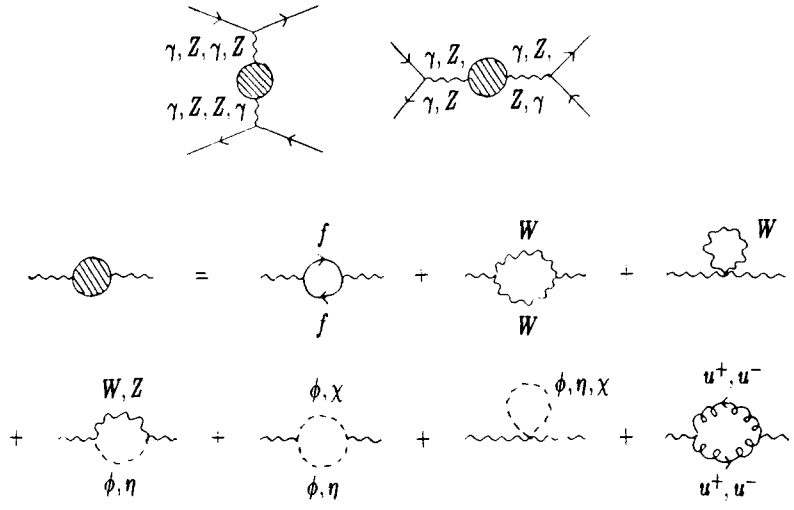

Fig. 8. Self-energy corrections.

4. Weak corrections

The weak corrections consist of one-loop diagrams with W, Z^0, Higgs and ghost lines. In this way the full structure of the standard model as a non-Abelian spontaneously broken gauge theory enters. Since in Bhabha scattering we deal only with very light fermions we may safely neglect the Yukawa couplings of the Higgs fields.

4.1. CORRECTING THE MATRIX ELEMENT

As already mentioned, at high energies the corrections can be written as multiplicative factors to the Born matrix element. The weak corrections [16] have the following form.

(a) The weak *self-energy corrections* consist of weak photon self-energy contributions (fermionic contributions to the photon self energy are already included in the electromagnetic corrections) as well as Z-self-energy and γ–Z mixing-energy contributions (fig. 8) ($r = \{s, t\}$)

$$\delta^{r\gamma}_{a;\mathrm{w},\Sigma}(\lambda) = \Pi^{\gamma}_{\mathrm{w}}(r) = -\hat{\Sigma}^{\gamma}_{\mathrm{w}}(r)/r,$$

$$\delta^{rZ}_{1;\mathrm{w},\Sigma}(\lambda) = \Pi^{Z}(r) + \frac{2}{g^{Z}_{\lambda}}\Pi^{\gamma Z}(r),$$

$$\delta^{rZ}_{\substack{2\\3};\mathrm{w},\Sigma}(\lambda) = \Pi^{Z}(r) + \left(\frac{1}{g^{Z}_{+}} + \frac{1}{g^{Z}_{-}}\right)\Pi^{\gamma Z}(r), \tag{4.1}$$

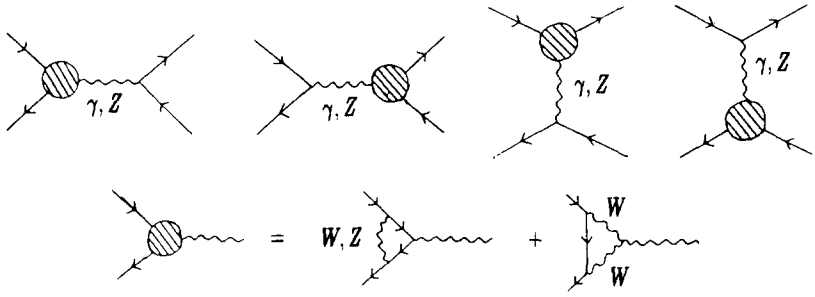

Fig. 9. Weak vertex corrections.

where

$$\Pi^{Z}(s) = \frac{s - M^2}{s - M_Z^2 + \hat{\Sigma}^{Z}(s)} - 1,$$

$$\Pi^{Z}(t) = \frac{t - M_Z^2}{t - M_Z^2 + \hat{\Sigma}^{Z}(t)} - 1,$$

$$\Pi^{\gamma Z}(r) = -\hat{\Sigma}^{\gamma Z}(r)/r. \tag{4.2}$$

The functions $\hat{\Sigma}^{Z}$ and $\hat{\Sigma}^{\gamma Z}$ are defined in ref. [16] and $\hat{\Sigma}^{\gamma}_{w}$ is given by

$$\hat{\Sigma}^{\gamma}_{w}(s) = \frac{\alpha}{4\pi}\left\{-\left(3s + 4M_W^2\right)F(s; M_W, M_W) + \tfrac{2}{3}s\right\}. \tag{4.3}$$

(b) The electron–gauge-boson vertex gets weak corrections from the diagrams shown in fig. 9 which lead to the *vertex corrections*

$$\delta^{ri}_{1,w,V}(\lambda) = 2F^{i}_{w}(r, \lambda), \tag{4.4}$$

$$\delta^{ri}_{\frac{2}{3},w,V}(\lambda) = F^{i}_{w}(r, +) + F^{i}_{w}(r, -). \tag{4.5}$$

The form factors F_w read

$$F^{\gamma}_{w}(s, -) = \frac{\alpha}{4\pi}\left\{\left(g^{Z}_{-}\right)^2 \Lambda_2\left(s, M_Z^2\right) + \frac{3}{2s_w^2}\Lambda_3\left(s, M_W^2\right)\right\}, \tag{4.6}$$

$$F^{\gamma}_{w}(s, +) = \frac{\alpha}{4\pi}\left\{\left(g^{Z}_{+}\right)^2 \Lambda_2\left(s, M_Z^2\right)\right\}, \tag{4.7}$$

$$F^{Z}_{w}(s, -) = \frac{\alpha}{4\pi}\left\{\left(g^{Z}_{-}\right)^2 \Lambda_2\left(s, M_Z^2\right) + \frac{1}{2s_w^2\left(2s_w^2 - 1\right)}\Lambda_2\left(s, M_W^2\right) - \frac{3c_w^2}{s_w^2\left(2s_w^2 - 1\right)}\Lambda_3\left(s, M_W^2\right)\right\}, \tag{4.8}$$

$$F^{Z}_{w}(s, +) = \frac{\alpha}{4\pi}\left\{\left(g^{Z}_{+}\right)^2 \Lambda_2\left(s, M_Z^2\right)\right\}, \tag{4.9}$$

where the functions Λ_2 and Λ_3 are given in ref. [16].

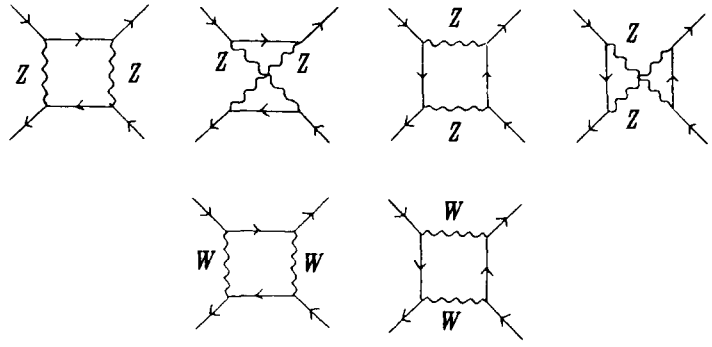

Fig. 10. Weak box diagrams.

(c) The evaluation of the weak *box diagrams* [27] (fig. 10) leads to the correction factors

$$\delta^{s\gamma}_{1,w,B}(\lambda) = \left(g^Z_\lambda\right)^4 C^{ZZ}_+(s,t) + \left(g^W_\lambda\right)^4 C^{WW}_+(s,t),$$

$$\delta^{s\gamma}_{2,w,B}(\lambda) = \left(g^Z_+\right)^2\left(g^Z_-\right)^2 C^{ZZ}_-(s,t),$$

$$\delta^{sZ}_{a,w,B}(\lambda) = 0. \tag{4.10}$$

The corrections of the t-channel boxes are obtained by substituting $s \leftrightarrow t$ and $2 \leftrightarrow 3$. The functions C can be decomposed in the following way

$$C^{ZZ}_\pm(s,t) = I^{ZZ}\left(s,t,M_Z^2\right) - I^{ZZ}\left(s,u,M_Z^2\right) \pm \left(I_5^{ZZ}\left(s,t,M_Z^2\right) + I_5^{ZZ}\left(s,u,M_Z^2\right)\right),$$

$$C^{WW}_+(s,t) = I^{ZZ}\left(s,t,M_W^2\right) + I_5^{ZZ}\left(s,t,M_W^2\right). \tag{4.11}$$

Again the explicit expressions for the functions I_5^{ZZ} and I^{ZZ} are given in ref. [16].

4.2. ORDER α^3 WEAK CORRECTIONS TO THE BHABHA CROSS SECTION

Collecting the weak one-loop results for the matrix elements gives as weak correction to the cross section

$$\delta\left(\frac{d\sigma}{d\Omega}\right)_{a,w,virt}(\lambda) = \frac{\alpha^2}{4s}\sum_{r,i,r',i'} \mathrm{Re}\left\{\mathscr{M}^{ri}_a(\lambda)\mathscr{M}^{r'i'*}_a(\lambda)\left[\delta^{ri}_{a,w}(\lambda) + \delta^{r'i'*}_{a,w}(\lambda)\right]\right\}, \tag{4.12}$$

with

$$\delta^{ri}_{a,\mathrm{w},\mathrm{virt}}(\lambda) = \delta^{ri}_{a,\mathrm{w},\Sigma}(\lambda) + \delta^{ri}_{a,\mathrm{w},\mathrm{V}}(\lambda) + \delta^{ri}_{a,\mathrm{w},\mathrm{B}}(\lambda). \tag{4.13}$$

This concludes the calculation of the (virtual and soft real) radiative corrections to the Bhabha cross section with longitudinally polarized initial beams. The final result is obtained by adding up the contributions of eqs. (2.6), (3.23) and (4.12)

$$\left(\frac{\mathrm{d}\sigma}{\mathrm{d}\Omega}\right)_a(\lambda) = \left(\frac{\mathrm{d}\sigma}{\mathrm{d}\Omega}\right)_{a,\mathrm{Born}}(\lambda) + \delta\left(\frac{\mathrm{d}\sigma}{\mathrm{d}\Omega}\right)_{a,\mathrm{em}}(\lambda) + \delta\left(\frac{\mathrm{d}\sigma}{\mathrm{d}\Omega}\right)_{a,\mathrm{w},\mathrm{virt}}(\lambda). \tag{4.14}$$

5. Numerical results and discussion

In sect. 3 we have given explicit analytical expressions for virtual electromagnetic and weak corrections and real soft photon bremsstrahlung. Adding hard photon emission yields the complete correction to the differential cross section of order α^3.

In this section we present the results of a numerical evaluation using the following set of parameters for the electroweak model

$$M_{\mathrm{Z}} = 93.0\ \mathrm{GeV}, \qquad M_{\mathrm{W}} = 82.1\ \mathrm{GeV}, \qquad \left(s^2_{\mathrm{w}} = 0.22\right). \tag{5.1}$$

Lepton masses are taken from ref. [28]. For the top quark mass we take $m_t = 35$ GeV, for the Higgs mass M_{H} we consider 100 GeV as a reasonable value. Since we have calculated the W and Z self-energies in the one-loop approximation only, we use the corresponding values for the widths of these particles

$$\Gamma_{\mathrm{Z}} = 2.538\ \mathrm{GeV}, \qquad \Gamma_{\mathrm{W}} = 2.537\ \mathrm{GeV}. \tag{5.2}$$

The soft bremsstrahlung is calculated with an energy cutoff $\Delta E = 0.05\sqrt{s}$ to the photon energy. The results for the electromagnetic corrections obtained here are approximate and will be supplemented in part II of this paper by hard bremsstrahlung effects.

5.1. SURVEY OF WEAK CORRECTIONS

In order to give an impression of the energy dependence of the different contributions to these corrections we present in table 1 our results for a scattering angle of 90° and energies from 44 to 1000 GeV. The numerical results for the cross section to order α^3 in different renormalization schemes should differ mostly by terms which are of the order of magnitude of the next order correction, if the same set of input data is used. This need not be true for the separate contributions. In order to make possible a detailed check of our calculations we present the numerical results for all of them separately. The electromagnetic corrections (em), given here with soft bremsstrahlung, are rather large but will become smaller outside the

TABLE 1
Radiative corrections at 90° scattering angle in permille of the Born cross section

$\sqrt{s}$/GeV	44	60	80	91	93	95	110	150	200	1000
em	−219.7	−223.7	−251.2	−441.5	−434.7	121.9	−205.9	−202.4	−197.2	−178.8
weak	−1.74	0.05	25.92	103.93	−10.47	74.90	−18.20	−41.33	−50.56	−128.48
Σ^Z	−1.57	0.37	27.51	111.52	−0.82	85.55	−16.62	−40.87	−48.85	−70.34
F^Z	−0.11	−0.38	−2.14	−9.59	−12.08	−13.23	−2.20	−0.32	−2.59	−36.76
rest	−0.07	0.05	0.54	2.00	2.43	2.58	0.62	−0.14	0.88	−21.38
$\Sigma^{\gamma Z}$	−0.07	−0.06	0.15	1.54	2.14	2.57	0.74	0.38	0.49	0.87
Σ^γ	−0.10	−0.18	−0.26	−0.08	−0.02	−0.02	−0.66	−1.38	−2.29	−12.47
F^γ	−0.06	−0.04	0.05	0.05	0.00	−0.05	0.16	0.93	1.72	4.63
C^{WW}	0.12	0.26	0.56	0.52	0.29	−0.03	0.00	−0.41	0.85	−13.26
C^{ZZ}	0.04	0.06	0.05	−0.02	0.01	0.10	0.38	0.33	0.11	−1.14

resonance region when hard photon emission is included. The weak corrections (weak) do not depend on experimental cuts but test the gauge theory character of the standard model. Therefore, the main interest of this paper lies on the discussion of these higher order weak effects. The most important contribution is the Z^0-boson self-energy (Σ^Z) which reaches about 10% of the Born cross section in the vicinity of the resonance. It is dominated by the fermion loop diagrams. All other weak corrections with exception of the Ze-vertex correction (F^Z) around the resonance give rather small (10^{-3}) contributions in the energy range up to 200 GeV. (Their sum is denoted by "rest" in table 1). If an accuracy of 1% is sufficient it is enough to take into account the Z^0 self-energy only. This allows a very simplified discussion of weak radiative corrections since their effect then is to replace, in the reduced propagator (2.4), the denominator by the corresponding complete expression. If, in addition, the Ze-vertex (3.25) is included an accuracy of 0.3% is obtained for energies up to 200 GeV. This is no more the case for energies which are large compared to M_Z, as can be seen from the results for 1000 GeV.

For further illustration of the importance of the separate weak corrections we show in fig. 11 and fig. 12 the contributions of the Z^0-self-energy, Ze-vertex and the rest of the weak corrections to the unpolarized differential Bhabha cross section, in the resonance region and above the resonance up to 1000 GeV.

5.2. ENERGY AND ANGULAR DEPENDENCE

(a) Small energies, $s \ll M_Z^2$.

At PETRA/PEP energies the weak contribution to the Born cross section is rather small. Therefore, we expect also tiny weak radiative corrections. This is confirmed by the results of the explicit calculations presented in fig. 13.

(b) Resonance region, $s \approx M_Z^2$.

In subsect. 5.1 we have seen that the weak corrections, in general, are dominated by the Z^0-self-energy correction. Since, on top of the resonance in an on-shell

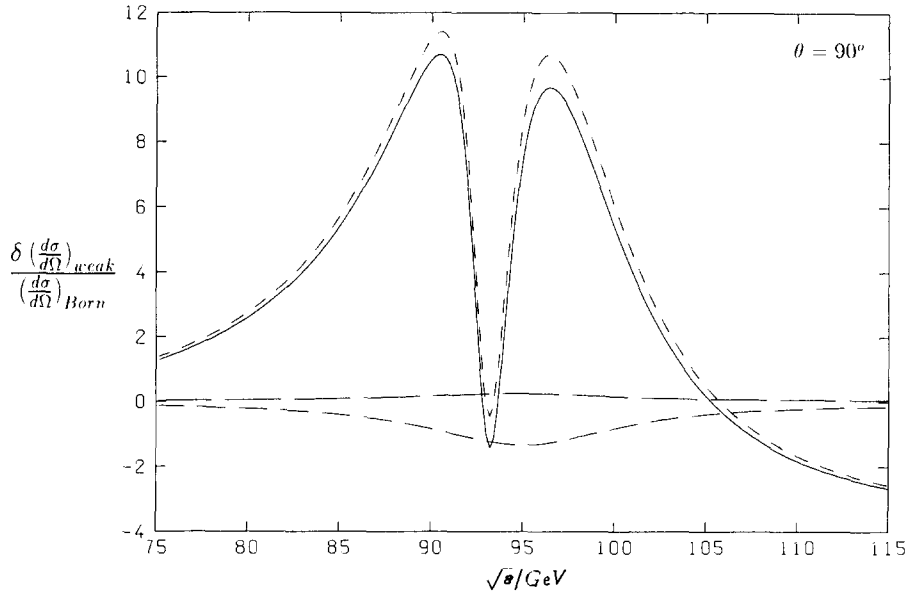

Fig. 11. Z^0 self-energy (small dashes), Ze-vertex (medium dashes), the rest of the weak corrections (long dashes) and their sum (solid line) to 90°Bhabha scattering in the resonance region as a percentage of the Born cross section.

renormalization scheme, the self-energy has to vanish, the weak corrections should be small. Fig. 14 shows that this is indeed the case. The situation is different already for energies 2 GeV above or below the resonance. With the exception of the forward direction the weak corrections lower considerably the differential cross section (see fig. 15). The energy dependence of the differential cross section at 90° in the Born approximation, including electromagnetic and weak corrections, is shown in fig. 16. The reduction by almost a factor of two will be partly compensated by inclusion of hard bremsstrahlung.

(c) High energies $s \gg M_Z^2$.

Fig. 17 shows the differential cross sections at 200 GeV. The weak corrections are important for scattering angles larger than 90° where they reduce the cross sections considerably. At even higher energies the weak corrections become as important as those which are electromagnetic. This can be explicitly seen in fig. 18 for 90° scattering.

5.3. SMALL ANGLE SCATTERING

The precise knowledge of the theoretical predictions for small angle scattering is of special importance since this enters the determination of the luminosity of e^+e^- storage rings. Bhabha scattering in the forward direction is dominated by the

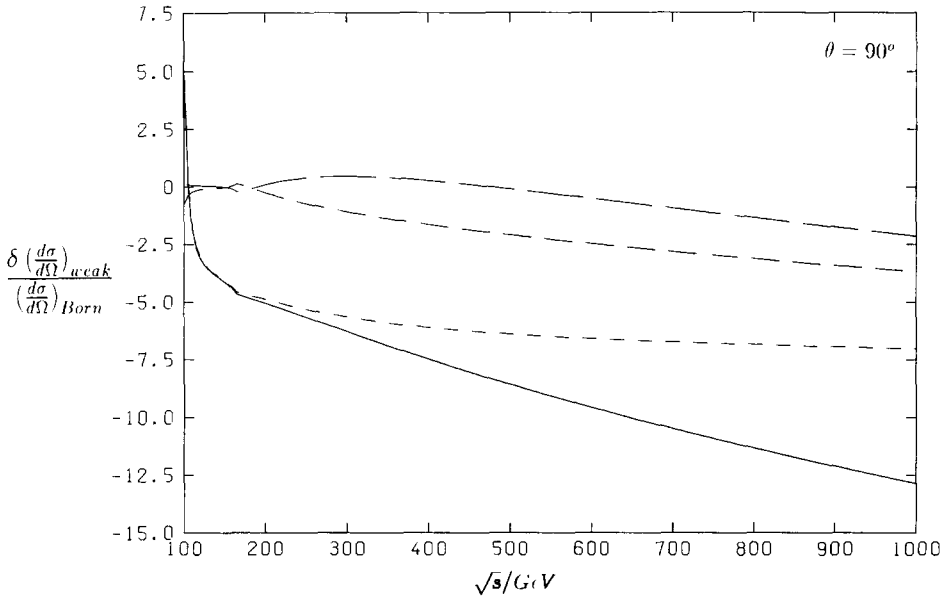

Fig. 12. Weak radiative corrections (in %) to 90° Bhabha scattering for 100 GeV $\leqslant \sqrt{s} \leqslant$ 1000 GeV (same signature as in fig. 11).

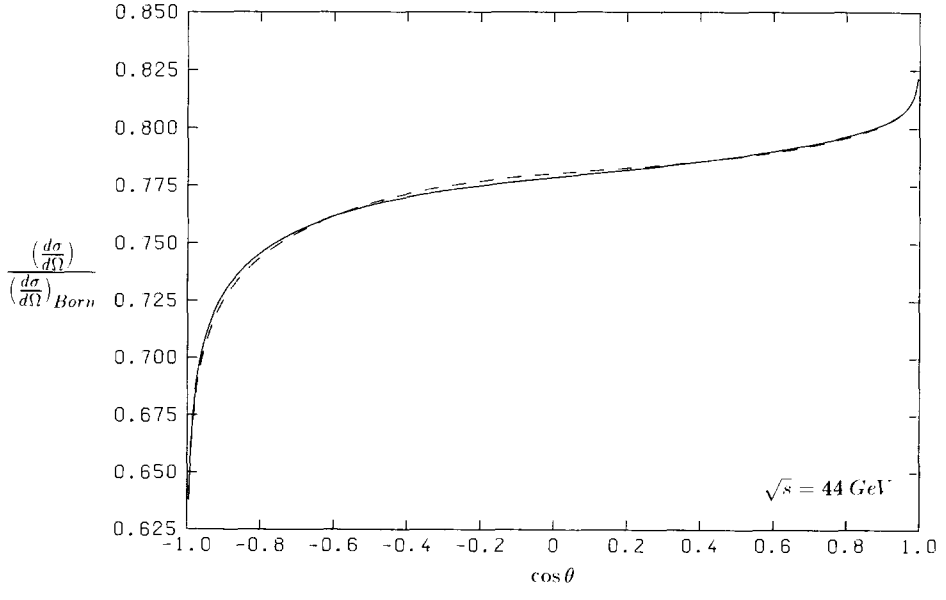

Fig. 13. Bhabha scattering at $\sqrt{s} = 44$ GeV. Differential cross section including electromagnetic (dashes) and total electroweak corrections (solid line) divided by the Born cross section.

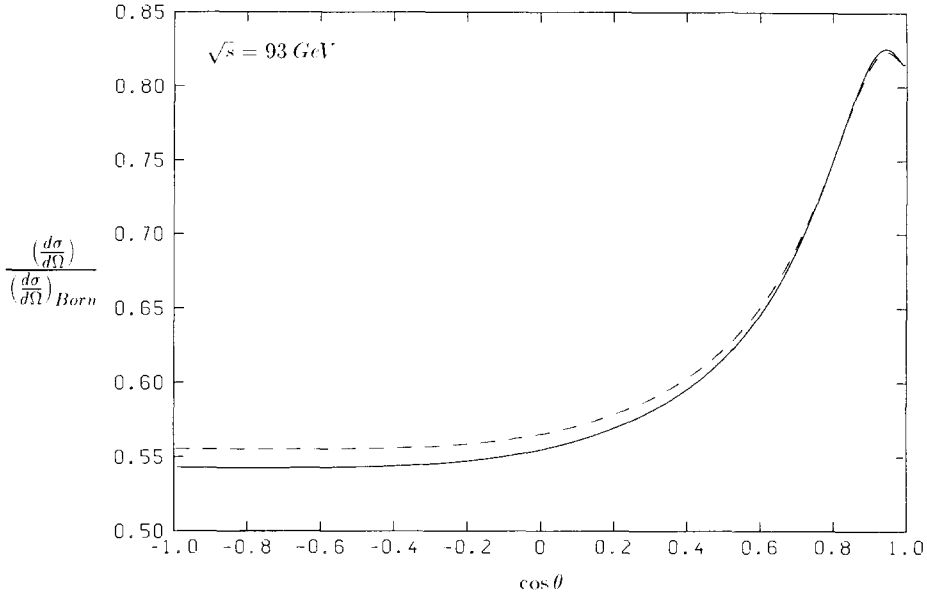

Fig. 14. Bhabha scattering at $\sqrt{s} = 93$ GeV (same signature as in fig. 13).

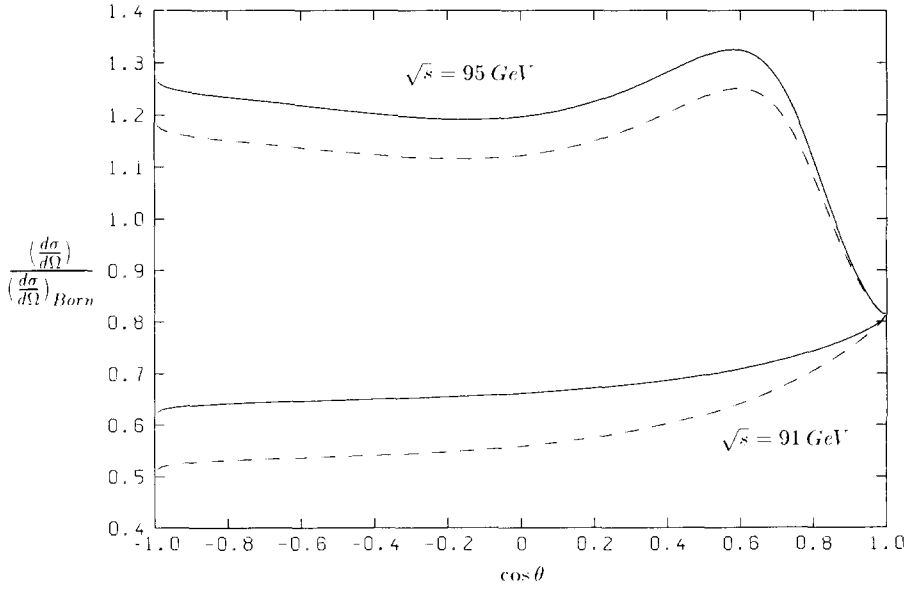

Fig. 15. Bhabha scattering at $\sqrt{s} = 91$ and 95 GeV (same signature as in fig. 13).

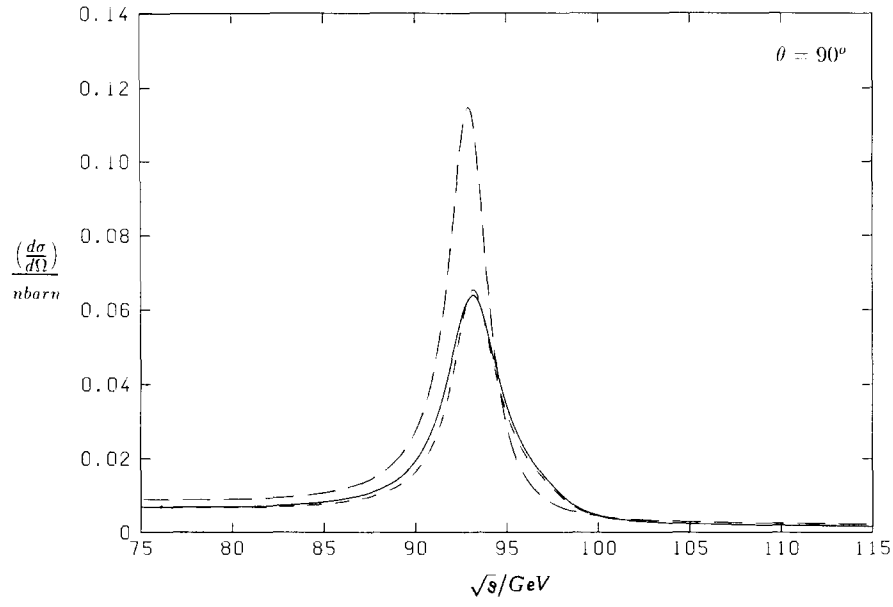

Fig. 16. Differential Bhabha cross section in the Born approximation (long dashes), with electromagnetic (short dashes) and with the total electroweak corrections (solid line) at 90°.

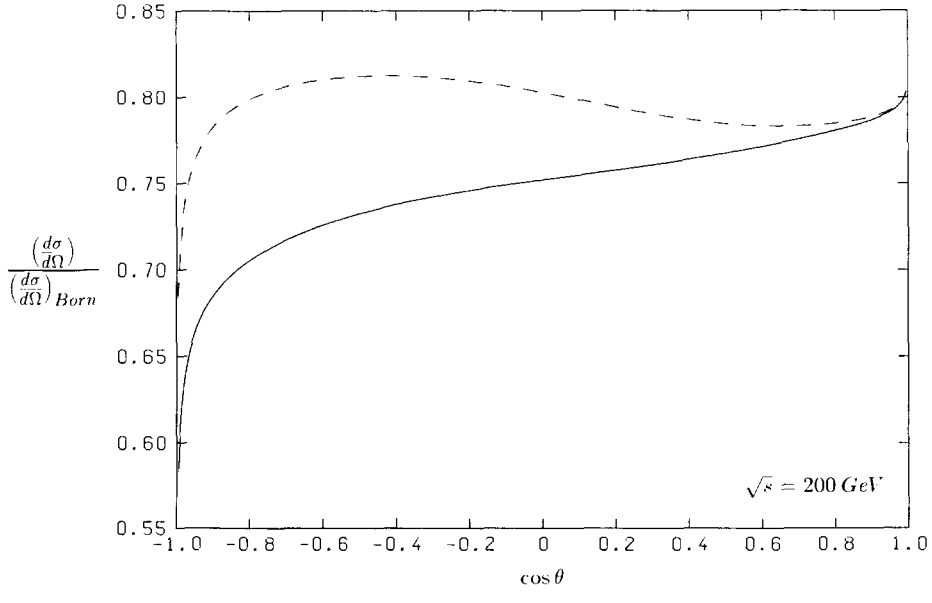

Fig. 17. Bhabha scattering at $\sqrt{s} = 200$ GeV (same signature as in fig. 13).

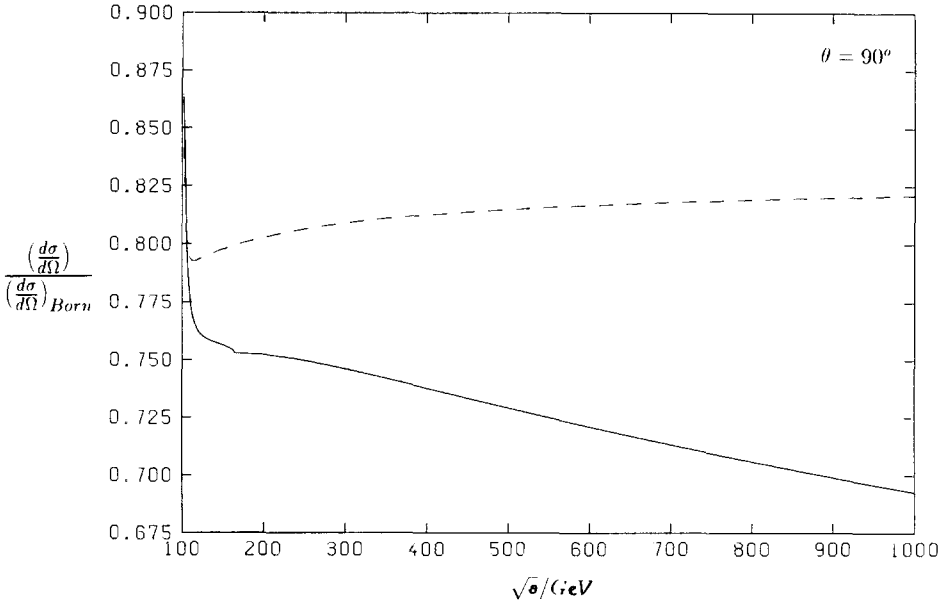

Fig. 18. Bhabha scattering at 90° in the energy range 100 GeV $\leqslant \sqrt{s} \leqslant$ 1000 GeV (same signature as in fig. 13).

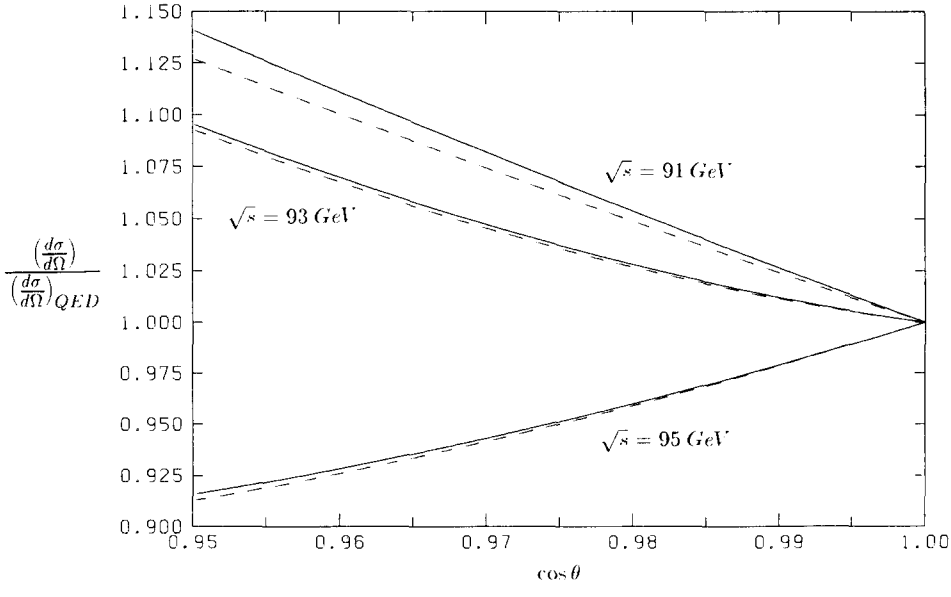

Fig. 19. Differential cross section including the electromagnetic (dashes) and the total electroweak corrections (solid line) divided by the electromagnetic cross section in the forward direction at $\sqrt{s}$ = 91, 93, 95 GeV.

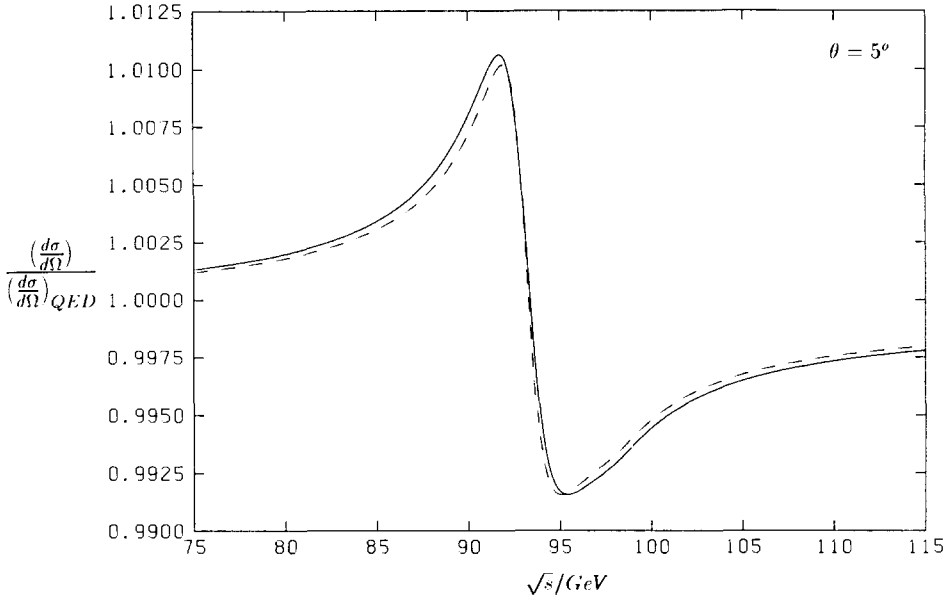

Fig. 20. Bhabha cross section at 5° scattering angle in the resonance region (same signature as in fig. 19).

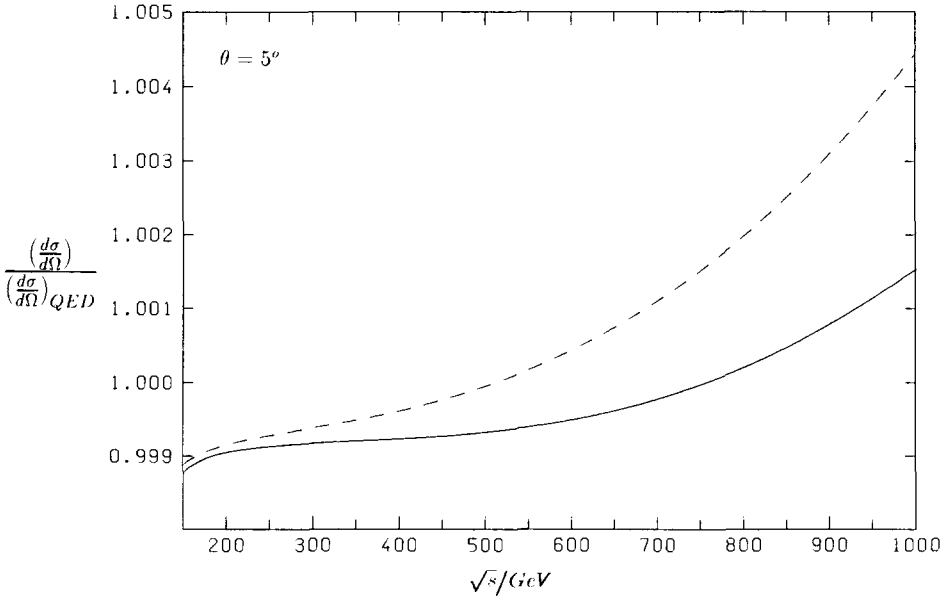

Fig. 21. Bhabha cross section at 5° scattering angle (same signature as in fig. 19).

t-channel γ-exchange matrix element. Therefore, we compare the effects of radiative corrections with the results of one-loop radiatively corrected pure QED. In the following figures we show the angular and energy dependence of the so defined relative corrections coming from Z^0-exchange and the corresponding photonic corrections and from purely weak radiative corrections.

In the resonance region these corrections vanish of course for $\theta \to 0$. In fig. 19 we present them for energies of 91, 93 and 95 GeV. For $\cos\theta \geqslant 0.97$ the corrections to pure QED amount to 8, 5, and -6%, respectively. For smaller angles they become smaller. We show the results for $\theta = 5°$ for energies between 75 and 115 GeV in fig. 20. They show the behaviour typical for a resonance and reach up to 1%. The weak corrections become more important at high energies also in the forward direction. This is shown in fig. 21 for a scattering angle of 5° and energies up to 1 TeV, but their absolute value remains smaller than 0.1%.

6. Conclusion

We have presented in this paper a complete set of analytical formulae for the one-loop electroweak corrections to Bhabha scattering without hard photon emission. The results of this paper are used as an input for Monte Carlo calculations of the two-particle cross section [17]. We have discussed the numerical values of the weak corrections for energies below, on top and far above the Z^0 resonance. Off resonance, the by far largest effect results from fermion-loop contributions to the Z^0 self-energy. The next important contributions are the weak vertex corrections which amount up to 1% around the Z^0 resonance. Since the Z^0-boson self-energy is subtracted on-shell, these vertex corrections become the dominant weak ones on the Z^0 peak. All other weak corrections remain smaller than 0.3% for energies up to 200 GeV. Here, we want to add a more general remark on the correction coming from the Z-boson self-energy: since the dominant effects (for m_t not too big) come from the light fermions, they can be absorbed into an improved tree-level cross section by replacing the fine structure constant α by

$$\alpha\left(M_W^2\right) = \frac{\alpha(0)}{1-\Delta r} = \frac{\sqrt{2}}{\pi} G_F M_W^2 \sin^2\theta_w , \tag{6.1}$$

(which is not the QED running α) which contains the large fermionic contributions via the radiative correction Δr to the μ lifetime (and therefore to the Fermi constant G_F), [29]. Then, the remaining weak corrections are everywhere of the order of a few percent (as long as no heavy particles or new physics contributions are considered). Theoretical uncertainties in the weak corrections from the hadronic vacuum polarization and unknown higher order effects, as estimated in ref. [30], result in an uncertainty of 0.0013 in the correction from the Z self-energy and of $\sim 0.3\%$ in the cross section. The electromagnetic corrections are rather large, in particular in the resonance region. In order to obtain results which are reliable within 1% a careful study of the leading contributions of higher loops is necessary.

References

[1] LEP Design Report, CERN-LEP/84-01 (1984)
[2] C.Y. Prescott, SLAC-PUB-2854 (1981);
Proc. SLAC-Workshop, SLAC-247 (1982)
[3] S. Weinberg, Phys. Rev. Lett. 19 (1967) 1264;
A. Salam, Proc. 8th NOBEL Symposium, S. 367, Stockholm, 1968, ed. N. Svartholm;
S.L. Glashow, J. Illiopoulos and L. Maiani, Phys. Rev. D2 (1970) 1285
[4] J. Ellis and R. Peccei, CERN Report Physics at LEP, CERN 86-02 and references therein
[5] H.J. Bhabha, Proc. Roy. Soc. 154A (1935) 159
[6] M.L.G. Readhead, Proc. Roy. Soc. 220A (1953) 219
[7] R.V. Polovin, ZhETF(USSR) 31 (1956) 449; JETP (Sov. Phys.) 4 (1957) 385;
Y.S. Tsai, Phys. Rev. 120 (1960) 269;
F.A. Berends, K.J.F. Gaemers and R. Gastmans, Nucl. Phys. B68 (1974) 541;
E. Calva-Tellez, Phys. Rev. D8 (1973) 3856;
W. Hollik, Phys. Lett. B123 (1983) 259
[8] D. Dicus, Phys. Rev. D8 (1973) 890;
R. Budny and A. Mcdonald, Phys. Rev. D9 (1974) 3107;
R. Budny, Phys. Lett. 55B (1975) 227
[9] W. Hollik and A. Zepeda, Z. Phys. C12 (1982) 67;
H.A. Olsen and P. Osland, Phys. Rev. D25 (1982) 2895
[10] M. Consoli, Nucl. Phys. B160 (1979) 208
[11] M. Consoli, S.Lo. Presti and M. Greco, Phys. Lett. B113 (1982) 415
[12] M. Greco, Phys. Lett. B177 (1986) 97
[13] M. Böhm, A. Denner, W. Hollik and R. Sommer, Phys. Lett. B144 (1984) 414
[14] K. Tobimatsu and Y. Shimizu, Prog. Theor. Phys. 75 (1986) 905
[15] B.W. Lynn, M.E. Peskin and R.G. Stuart, SLAC-PUB-3725 (1985)
[16] M. Böhm, W. Hollik and H. Spiesberger, Fortschr. Phys. 11 (1986) 687
[17] F.A. Berends, R. Kleiss and W. Hollik, Nucl. Phys. B304 (1988) 712
[18] F.A. Berends, R. Kleiss, P. De Causmaecker, R. Gastmans, W. Troost and T.T. Wu, Nucl. Phys. B206 (1982) 53;
P. De Causmaecker, R. Gastmans, W. Troost and T.T. Wu, Nucl. Phys. B206 (1982) 61
[19] F.A. Berends,K.J.F. Gaemers and R. Gastmans, Nucl. Phys. B57 (1973) 381; B63 (1973) 381
[20] I.B. Khriplovich, Sov. J. Nucl. Phys. 17 (1973) 298;
R.W. Brown, V.K. Chung, K.O. Mikaelian and E.A. Paschos, Phys. Lett. B43 (1973) 403;
A.B. Kraemmer and B. Lautrup, Nucl. Phys. B95 (1975) 380;
F.A. Berends and G.J. Komen, Nucl. Phys. B115 (1976) 114
[21] M. Böhm and W. Hollik, Nucl. Phys. B204 (1982) 45;
R.W. Brown, R. Decker and E.A. Paschos, Phys. Rev. Lett. 52 (1984) 1192;
M. Consoli and A. Sirlin, *in* Physics at LEP, vol. 1, CERN report (1986) p. 63
[22] R. Lewin, Dilogarithms and associated functions (London, 1958)
[23] F. Jegerlehner, Z. Phys. C32 (1986) 195
[24] F.A. Berends and G.J. Komen, Phys. Lett. B63 (1976) 432;
E.A. Paschos, Nucl. Phys. B159 (1979) 285;
W. Wetzel, Z. Phys. C11 (1981) 117;
J. Cole, G. Penso and C. Verzegnassi, Trieste preprint 19/85/EP;
B.W. Lynn, G. Penso and C. Verzegnassi, SLAC-PUB-3742 (1985)
[25] F. Jegerlehner, private communication
[26] M. Greco, G. Pancheri-Srivastava and Y. Srivastava, Nucl. Phys. B101 (1975) 234; B171 (1980) 118
[27] A. Denner, Diploma Thesis, Würzburg (1984)
[28] Particle Data Group, Phys. Lett. B170 (1986) 116
[29] A. Sirlin, Phys. Rev. D22 (1980) 971
[30] F. Jegerlehner, Z. Phys. C32 (1986) 425